Sensors and Materials, Vol. 18, No. 8 (2006) 433–444
MYU Tokyo

S & M 0661

Determination of Electrical Properties of n-Type and p-Type Polycrystalline Silicon Thin Films as Sensor Materials

Hideo Muro*, Takeshi Mitamura[1] and Shigeyuki Kiyota[2]

Department of Electrical, Electronics and Computer Engineering, Chiba Institute of Technology, 2-17-1 Tsudanuma, Narashino, Chiba 275-0016, Japan
[1]Nissan Research Center, Nissan Motor Co., Ltd., 1 Natsushima-cho, Yokosuka, Kanagawa 237-8523, Japan
[2]Powertrain Engineering Division, Nissan Motor Co., Ltd., 1-1 Morinosatoaoyama, Atsugi, Kanagawa 243-0123, Japan

(Received October 25, 2006; accepted December 7, 2006)

***Key words*:** polycrystalline silicon, microsensor, piezoresistive, thermoelectric

The electrical properties of both n-type and p-type polycrystalline silicon (polysilicon) films for sensor applications have been characterized, together with the basic electrical characteristics of these films. For n-type and p-type polysilicon piezoresistors, the measured longitudinal gauge factors are –15 to –24 and 24 to 31, respectively, whereas the transverse gauge factors are much smaller. The temperature coefficients of resistance are between –1000 and –2000 ppm/K for both n-type and p-type polysilicons. A full-bridge configuration for stress sensors using both n-type and p-type polysilicon piezoresistors is proposed. The measured Seebeck coefficients for n-type and p-type polysilicon films are –0.21 to –0.43 mV/K and 0.21 to 0.28 mV/K, respectively.

1. Introduction

Polycrystalline silicon (polysilicon) thin films deposited by low-temperature chemical vapor deposition (LPCVD) are widely used as gate materials of metal-oxide semiconductor field-effect transistors (MOSFETs) and resistors in integrated circuits. The electrical properties such as the resistivity and Hall mobility of polysilicon films have been intensively studied and analyzed.[1–4] With advances in micro-electro-mechanical systems (MEMS) technology, the applications of polysilicon thin films have been extended to silicon sensors as piezoresistive gauges[5–8] or thermocouples[9–12] due to their comparatively large piezoresistive coefficients and Seebeck coefficients, in addition to their insulator-isolated structures for high-temperature operation or thermal isolation. Polysilicon thermoelectric detectors with thermally isolated structures realized using silicon micromachining technology can be applied not only for infrared sensors,[9–12] but also for mass flow sensors[13,14] or vacuum sensors.

*Corresponding author, e-mail address: hideo.muro@it-chiba.ac.jp

Insulator-isolated sensing elements can also be formed using silicon-on-insulator (SOI) technology where single-crystal silicon devices with high performances are available, although they are more expensive and less compatible with IC technology. In contrast, polysilicon sensing elements can be realized by a standard large-scale integration (LSI) process without any additional fabrication steps and easily incorporated into signal processing circuitry. The characteristics of polysilicon sensing elements, however, are considerably dependent on the fabrication process, and their determination is essential for designing sensors with sufficient reliability. The determination of the sensing properties of polysilicon films has been performed.[15–18] Most studies investigated only p-type polysilicon films and some dealt with polysilicon films that are not compatible with the standard IC process.

In this study, the gauge factors and Seebeck coefficients of both n-type and p-type polysilicon thin films formed by a conventional IC process have been systematically evaluated, together with the basic electrical properties of these films. In addition, by considering the measured results, the possibile complementary sensor configurations using both n-type and p-type polysilicon resistors are proposed.

2. Materials and Methods

2.1 *Test samples*

Test devices for evaluating the sensing properties of polysilicon films were designed, together with their mask patterns. The masks included resistors for evaluating the resistivity and piezoresistive coefficient, Hall elements for evaluating the Hall mobility and a specific test chip for evaluating the Seebeck coefficient. The length L and the width W of the resistors are 160 and 40 μm, respectively, resulting in an L/W ratio of 4. The Hall plates were 1-mm-long, 0.5-mm-wide rectangles with a pair of protruding highly doped output regions, as shown in Fig. 1. The test chip for measuring the Seebeck coefficients consisted of the polysilicon thermocouples to be evaluated, heaters for generating a temperature gradient across the chip and diodes for monitoring the temperatures on both sides of the chip. The whole chip layout is shown in Fig. 2.

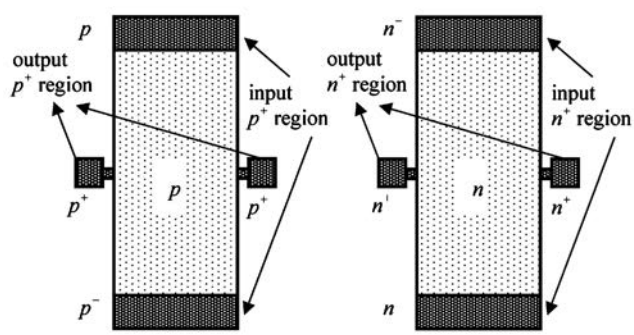

Fig. 1. Schematic drawings of (a) p-type and (b) n-type polysilicon Hall plates.

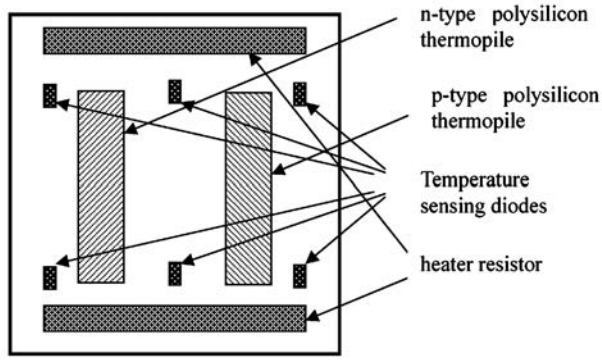

Fig. 2. Layout of test chip for measuring Seebeck coefficients of polysilicon thermopiles.

The test samples were fabricated by a conventional IC process. The starting material is a 5 inch, p-type silicon wafer with a 12 μm-thick 2 Ω·cm n-type epitaxial layer. After forming a 580-nm-thick initial oxide layer, a p-type isolation layer, a p-type base layer and an n-type emitter layer were diffused consecutively to integrate bipolar devices in the chip. Next, a 350-nm-thick polysilicon layer was deposited by LPCVD at 625°C and doped selectively by ion implantation using a photoresist as a mask. Phosphorus and boron were implanted to form n-type and p-type regions, respectively, with a dose ranging from 5×10^{14} to 5×10^{15}/cm^2. The implant energies were 100 and 40 keV for phosphorus and boron, respectively. After patterning the polysilicon layer by dry etching, it was thermally oxidized to form a 100-nm-thick buffer oxide layer and annealed for 30 min at 900°C to activate the implanted dopants. A 700-nm-thick silicon oxide layer was deposited by chemical vapor deposition (CVD), and contact holes were etched. Finally, a 1-μm-thick aluminum layer was deposited and patterned to form interconnections, and sintered in H_2.

2.2 *Measurements*

The fabricated test chips for evaluating the resistivity and Hall mobility of the polysilicon films were diced and mounted on ceramic packages with epoxy glue. The sample Hall plates were fixed in the 10-mm-wide gap of an electromagnet, and the Hall voltage, V_H, was measured by applying a uniform magnetic field, B, of 1 kG and biasing the input regions at a constant voltage, V_C, of 10 V. The effective Hall mobility, μ_H, was obtained using the relation $\mu_H = L\,V_H / WV_CB$, where W and L are the width and length of the Hall plates, respectively.

The samples for measuring the piezoresistance of the polysilicon films were carved out from the fabricated wafer in the form of a 70-mm-long and 1-mm-wide bar by dicing, and bonded on an alumina substrate, where one side of the bar was fixed on the substrate and the other side protruded from the substrate so that the distance between the piezoresistor and the edge of the substrate, d_1, was 13 mm. The substrate was incorporated into the experimental setup for measuring piezoresistance, as shown in Fig. 3, where the tip of the bar was pushed up by a lever driven by a stepping motor through a micrometer. The distance between the loading point and the edge of the substrate, d_2, was adjusted to 40 mm. When the deflection of the loading point is given by x, the surface stress along the silicon bar at the point of the piezoresistors, σ, can be calculated using

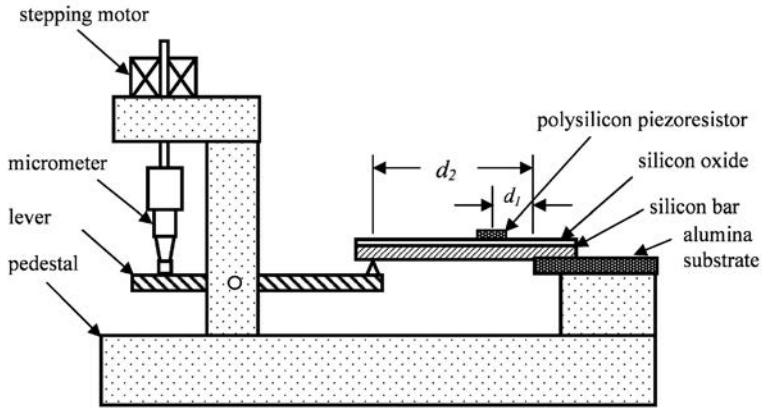

Fig. 3. Experimental setup for measuring gauge factors of polysilicon resistors formed on silicon bar-figured substrate.

$$\sigma = \frac{3Eh}{2{d_2}^3}(d_2 - d_1)x, \tag{1}$$

where E and h are theYoung's modulus and thickness of the silicon substrate, respectively.

The longitudinal and transverse gauge factors, G_l and G_t, respectively, can be calculated using the measured resistance-change ratios of the longitudinally and transversely directed polysilicon piezoresistors, $\delta R_l / R_l$ and $\delta R_t / R_t$, respectively, by

$$G_l = \frac{\delta R_l}{R_l} \cdot \frac{E}{\sigma}, \tag{2}$$

$$G_t = \frac{\delta R_t}{R_t} \cdot \frac{E}{\sigma}. \tag{3}$$

The test chip for measuring the Seebeck coefficient was mounted on a ceramic package where only one side of the test chip was bonded to a pedestal chip that had been bonded in the package for thermal isolation. The temperature difference δT was created by driving the heater on one side, which was measured using two calibrated diodes located on both sides of the chip. The resultant thermal resistance was about 8 K/W. The Seebeck coefficient was obtained by dividing the measured output voltage of the polysilicon thermopile by δT and the number of thermocouples comprising the thermopile.

3. Results and Discussion

3.1 *Resistivity*

The dependences of the resistivities of the fabricated p-type and n-type polysilicon resistors on doping concentration, together with those of single-crystal silicon, are shown in Fig. 4. The resistivities are calculated by multiplying the measured sheet resistances by the thickness of the polysilicon film, t. The measured results of the p-type polysilicon resistors are similar to those in refs. 15 and 17, although the values are slightly larger due to the smaller thickness of the film. At lower doping concentrations, the resistivity of the n-type polysilicon resistors is higher than that of the p-type polysilicon resistors and decreases rapidly with doping concentration, which seems to be due to the numerous electron traps in the grain boundaries.

The temperature dependences of the resistivities of the n-type and p-type polysilicon resistors are shown in Figs. 5 and 6, where the ordinates are the logarithms of the measured resistivities normalized by the values at 100°C and the abscissas are $1/kT$, where k and T are the Boltzmann constant and absolute temperature, respectively. The temperature coefficients are negative at lower doping concentrations and decrease to zero as doping concentration increases for both n-type and p-type polysilicon resistors. The temperature coefficients are –6000 to 170 ppm/K and –5000 to 0 ppm/K for the n-type and p-type polysilicon films, respectively.

The electrical properties of polysilicon resistors can be described by the carrier-trapping model. When the voltage across the undepleted crystallite is negligible due to sufficient doping, the entire applied voltage is consumed at each grain boundary junction, and the I-V characteristics can be approximately expressed as follows[2]

$$I = 2qnWt\sqrt{\frac{kT}{2\pi m^*}}\exp\left(-\frac{qV_B}{kT}\right)\sinh\left(\frac{qLV}{2kTL_g}\right). \tag{4}$$

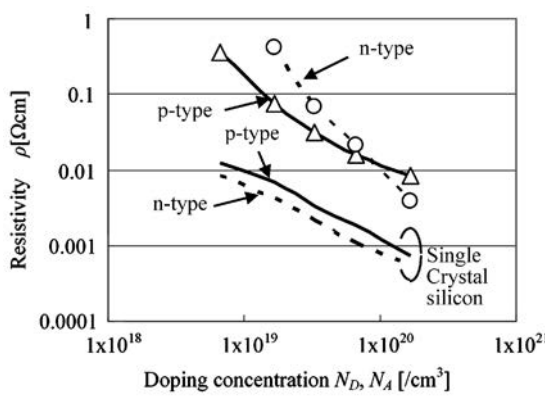

Fig. 4. Dependences of resistivities of fabricated p-type and n-type polysilicon resistors on doping concentration.

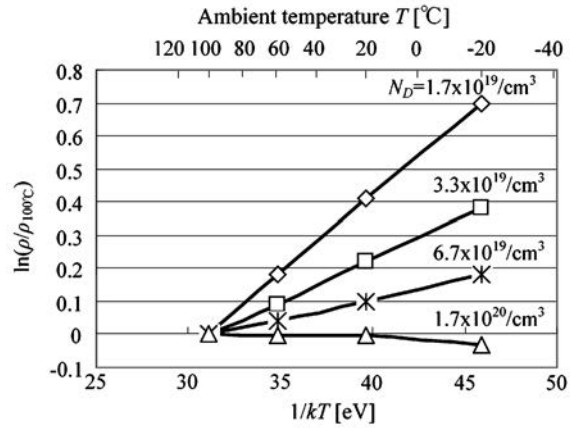

Fig. 5. Temperature dependences of measured resistivities of n-type polysilicon resistors normalized by the resistivity at 100°C with doping concentration as the parameter.

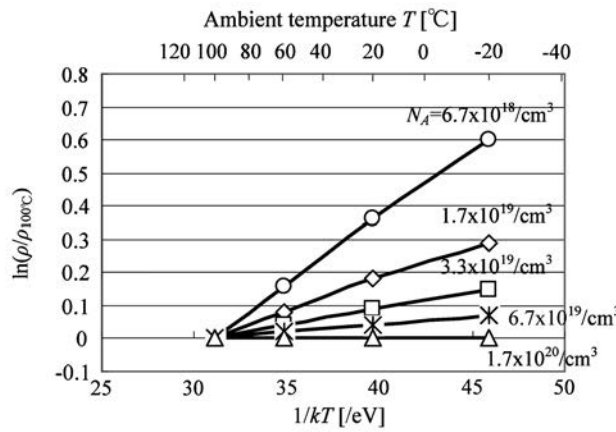

Fig. 6. Temperature dependences of measured resistivities of p-type polysilicon resistors normalized by the resistivity at 100°C with doping concentration as the parameter.

Here, q, n, m^*, V_B and L_g are the electron charge, average carrier concentration, effective mass of the carrier, potential barrier height and grain size, respectively. V_B is expressed using the trap density Q_t and the doping concentration N.

$$V_B = \frac{qQ_t^2}{8\varepsilon N}. \tag{5}$$

Here, ε is the dielectric permittivity of silicon.

When the applied voltage is small, the resistivity $\rho = tWV / LI$ is expressed using eq. (4) as

$$\rho = \frac{1}{q^2 n L_g} \sqrt{2\pi m^* kT} \exp\left(\frac{qV_B}{kT}\right). \tag{6}$$

From eq. (6), the slope of each line in Figs. 5 and 6 approximately represents the potential barrier height. Figure 7 shows the potential barrier height V_B, calculated from Figs. 5 and 6 as a function of the doping concentration, N_A or N_D. The potential barrier height V_B is inversely proportional to the doping concentration, as expressed in eq. (5), and the V_B of n-type polysilicon is higher than that of p-type polysilicon. The corresponding trap densities evaluated from eq. (5) are 6.3×10^{12} and 3.9×10^{12}/cm^2 for the n-type and p-type polysilicon resistors, respectively.

3.2 *Hall mobility*

Figure 8 shows the effective Hall mobilities of the n-type and p-type polysilicon films, which were calculated from the Hall voltages measured on the Hall plates biased at a constant voltage of 10 V under an applied magnetic field of 1 kG. The effective Hall mobilities of polysilicons are lower than those of single-crystal silicon by one or two orders of magnitude and increase with doping concentration for both n-type and p-type polysilicons. The effective Hall mobility of the n-type polysilicon increases more rapidly than that of the p-type polysilicon and finally begins to decrease at a doping level of approximately 1×10^{20} /cm^3.

3.3 *Gauge factors*

The temperature dependences of the longitudinal gauge factor G_l and the transverse gauge factor G_t of both the n-type and p-type polysilicon piezoresistors with doping concentration as a parameter are shown in Figs. 9 and 10, respectively. The gauge factors at 20°C are plotted again as functions of doping concentration in Fig. 11. The longitudinal

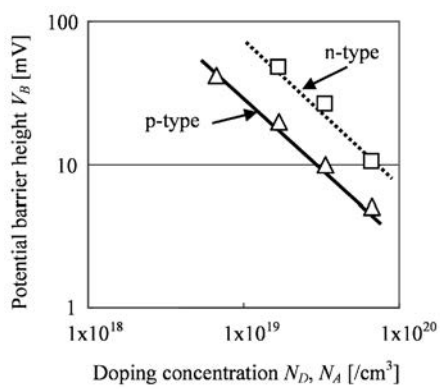

Fig. 7. Dependences of potential barrier heights of n-type and p-type polysilicon films on doping concentration N_D or N_A.

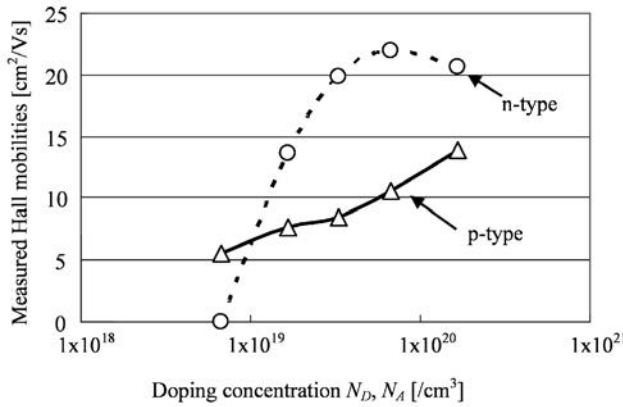

Fig. 8. Dependences of effective Hall mobilities of fabricated p-type and n-type polysilicon Hall plates on doping concentration.

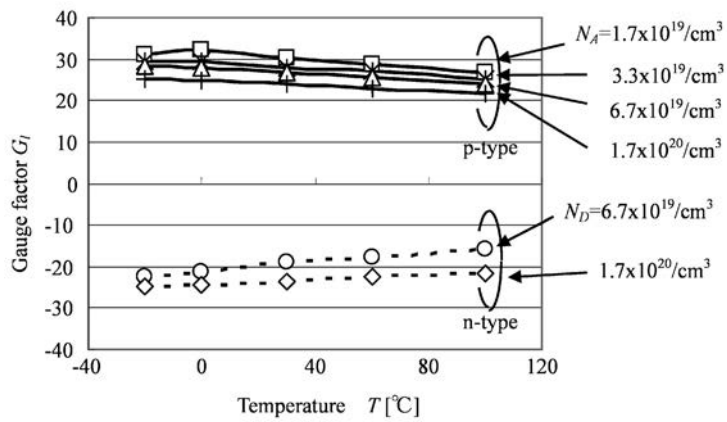

Fig. 9. Temperature dependences of measured longitudinal gauge factor, G_l, of n-type and p-type polysilicon piezoresistors with doping concentration as the parameter.

gauge factors of the n-type and p-type polysilicon piezoresistors are negative and positive, respectively, while the transverse gauge factors are positive and negative. The magnitude of the longitudinal gauge factor of the p-type polysilicon piezoresistors decreases from 31 to 24 with doping concentration, which is several times as large as that of the transverse one and about one-third as large as that of single-crystal silicon. For the n-type polysilicon piezoresistors, the magnitude of the longitudinal gauge factor decreases from 24 to 15 with doping concentration, which is more than one order of magnitude larger than that of the transverse one. The temperature coefficients lie between –1000 and –2000 ppm/K for both the n-type and p-type polysilicon piezoresistors. Only the transverse gauge factor of the n-

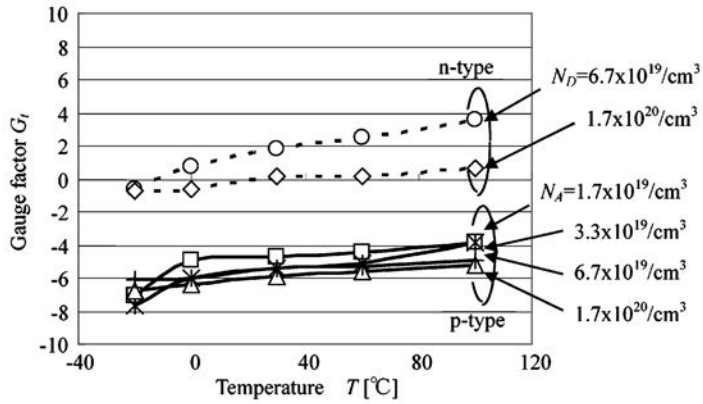

Fig. 10. Temperature dependences of measured transverse gauge factor, G_t, of n-type and p-type polysilicon piezoresistors with doping concentration as the parameter.

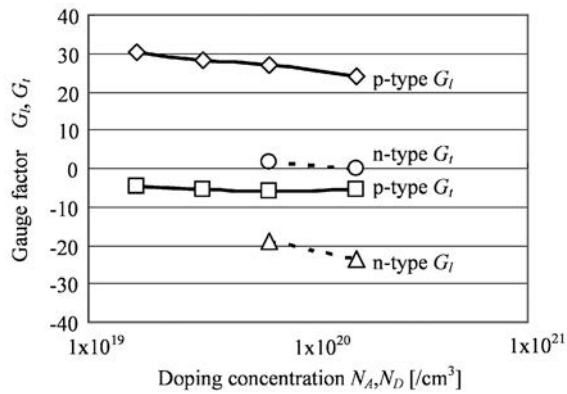

Fig.11. Dependences of measured longitudinal and transverse gauge factors, G_l and G_t, of fabricated p-type and n-type polysilicon piezoresistors on doping concentration.

type polysilicon piezoresistors has a positive temperature coefficient of about 2000 ppm/K, although its magnitude is small. Although some features of polysilicon piezoresistors were successfully analyzed using simplified polysilicon models,[14,18] they are considerably dependent on the fabrication process details and the resultant physical conditions of polysilicon grain boundaries, and can not be fully explained by such simple models.

Several stress sensors with polysilicon resistors have been developed using only p-type piezoresistors,[5,17] which impose considerable constraints on their design and applications. The fact that n-type and p-type polysilicon piezoresistors fabricated through a conventional IC process have significant longitudinal gauge factors with opposite signs implies the

possibility of integrating complementary polysilicon piezoresistors to form full-bridge stress sensors without any significant geometrical restrictions. Figure 12 shows some examples of the proposed stress sensor configurations. The layout of the polysilicon stress sensor shown in (a) is for sensors on beams that can be applied for accelerometers or stress monitors for the mechanical feedback control of resonators, whereas that shown in (b) is for sensors on diaphragms that can be applied for pressure sensors. A full-bridge sensor can be made compact in any direction, resulting in an optimal design by locating the sensors at maximum stress points.

3.4 *Seebeck coefficient*

Figure 13 shows the temperature dependences of the measured Seebeck coefficients of the n-type and p-type polysilicon resistors obtained by dividing the thermoelectric voltage of the polysilicon/aluminum thermocouple by the temperature difference. The Seebeck coefficient of n-type polysilicon is negative and its magnitude decreases from 0.43 to 0.21 mV/K with increasing doping concentration, while that of p-type polysilicon is positive and its magnitude decreases from 0.28 to 0.21 mV/K with increasing doping concentration. Although these values are about one-third of those of single-crystal silicon, these polysilicon films are still attractive as a material of thermopile sensors considering their inherent thermally and electrically isolated structures. The temperature coefficients of the Seebeck coefficient are about 1200 ppm/K for the n-type polysilicon and 500 to 1500 ppm/K depending on doping concentration for the p-type polysilicon. The n-type and p-type polysilicon films have similar Seebeck coefficients with opposite signs, and the sensitivity of the thermopile sensors consisting of both n-type and p-type polysilicon films[19] is more than twice as high as those using either of the polysilicon films. These thermopile sensors have an advantage for use in integrated sensors where on-chip signal processing is essential, such as infrared imagers and thermal sensors with temperature compensation.

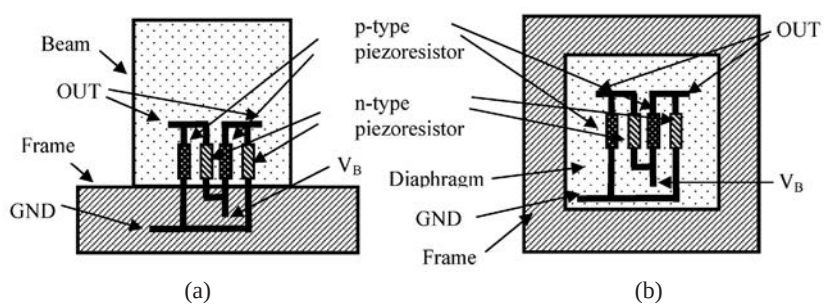

Fig. 12. Full-bridge stress sensor layout consisting of polysilicon piezoresistors formed on (a) beam and (b) diaphragm where interconnections are shown by thick lines and "GND," "V_B" and "OUT" are a minus input terminal, a plus input terminal and an output terminal, respectively.

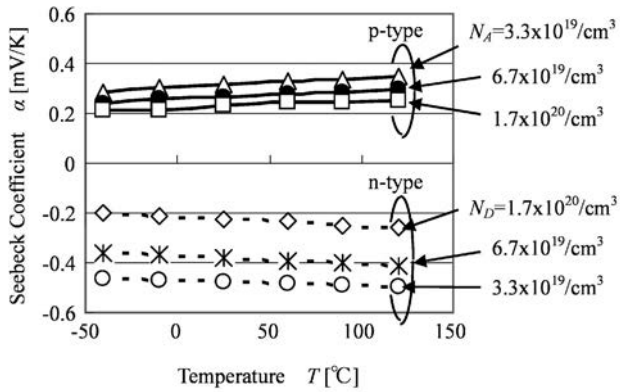

Fig. 13. Temperature dependences of measured Seebeck coefficients, α, of n-type and p-type polysilicon piezoresistors with doping concentration as the parameter.

4. Conclusions

Test chips for evaluating the electrical properties of both n-type and p-type polysilicon resistors for sensor applications have been designed and fabricated using a conventional IC process. The resistivities of the resistors are determined and the activation energies calculated from the temperature coefficients of the resistivities are applied to the carrier-trapping model to estimate the trap density at polysilicon grain boundaries. The effective Hall mobility was measured using polysilicon Hall plates in a magnetic field. It increased with doping concentration, and the mobility of n-type polysilicon was more dependent on doping concentration than that of p-type polysilicon. The longitudinal and transverse gauge factors were evaluated using bar-form test chips and a loading setup. The longitudinal gauge factors of the n-type and p-type polysilicon piezoresistors were –15 to –24 and 24 to 31, respectively, whereas the transverse gauge factors were much smaller. The temperature coefficients were between –1000 and –2000 ppm/K for both n-type and p-type polysilicon. A full-bridge configuration for stress sensors using both n-type and p-type polysilicon piezoresistors complementarily is proposed. The Seebeck coefficient was measured using test chips incorporating polysilicon thermocouples, heaters and temperature-sensing diodes. The measured Seebeck coefficients of n-type and p-type polysilicon films were –0.21 to –0.43 mV/K and 0.21 to 0.28 mV/K, respectively. These experimental results seem to be helpful in designing polysilicon sensors, particularly in complementary configurations; however, they considerably depend on the fabrication process, and specific characterizations for each development are essential.

Acknowledgement

The authors would like to thank members of the Nissan Research Center for their help in the fabrication of the devices.

References

1 J. Y. W. Seto: J. Appl. Phys. **46** (1975) 5247.
2 N. C. Lu, L. Gerzberg, C. Lu and J. D. Meindl: IEEE Trans. Electron Devices **28** (1981) 818.
3 T. I. Kamins: J. Appl. Phys. **42** (1971) 4357.
4 M. E. Cowher and T. O. Sedgwick: J. Electrochem. Soc. **119** (1972) 1565.
5 V. Mosser, J. Suski, J. Goss and E. Obermeier: Sens. Actuators, A **28** (1991) 113.
6 H. Schäfer, V. Graeger and R. Kobs: Sens. Actuators, **17** (1989) 521.
7 H. Guckel and D. W. Burns: Transducers'85, 3rd Int. Conf. on Solid-State Sensors and Actuators, Philadelphia (1985) p. 182.
8 S. Sugiyama, T. Suzuki, K. Kawahata, M. Takigawa and I. Igarashi: Proc. 6th Sensor Symp. (1986) p. 23.
9 G. R. Lahiji and K. D. Wise: IEEE Trans. Electron Devices **29** (1982) 14.
10 P. M. Sarro, A. W. Herwaarden and W. van der Vlist: Sens. Actuators, A **41** (1994) 666.
11 R. Lenggenhager, H. Baltes, J. Peer and M. Forster: IEEE Electron Device Lett. **13** (1992) 454.
12 E. Socher, O. B.-Degani and Y. Nemirovsky: J. Microelectromech. Syst. **9** (2000) 38.
13 M. Parameswaran, A. M. Robinson, Lj. Ristic, K. Chau and W. Allegretto: Sensors and Materials **2** (1990) 17.
14 D. Moser, R. Lenggenhager and H. Baltes: Sens. Actuators, A **25** (1991) 577.
15 M. Le Berre, M. Lemiti, D. Barbier, P. Pinard, J. Cali, E. Bustarret, J. Sicart and J. L. Robert: Sens. Actuators, A **46** (1995) 166.
16 V. A. Voronin, A. A. Druzhinin, I. I. Marjamova, V. G. Kostur and J. M. Pankov: Sens. Actuators, A **30** (1992) 143.
17 E. Obermeier and P. Kopystynski: Sens. Actuators, A **30** (1992) 149.
18 D. Schubert, W. Jenschke, T. Uhlig and F. M. Schmidt: Sens. Actuators **11** (1987) 145.
19 H. Muro, T. Mitamura and C. J. Schaeffer: T. IEE Japan **112-A** (1992) 968.